Editors' Suggestion Featured in Physics

Capturing Rainbow in On-Chip Phononic Crystals

Riyi Zheng,[1] Weijian Xie,[1] Xinhua Wen,[1] Weiyin Deng,[2,*] Manzhu Ke,[2] Jiuyang Lu,[2,†] Xueqin Huang,[1,‡] and Zhengyou Liu[2,3,§]

[1]*School of Physics and Optoelectronics, South China University of Technology, Guangzhou 510640, China*

[2]*Key Laboratory of Artificial Micro- and Nanostructures of Ministry of Education and School of Physics and Technology, Wuhan University, Wuhan 430072, China*

[3]*Institute for Advanced Studies, Wuhan University, Wuhan 430072, China*

(Received 3 February 2026; revised 25 May 2026; accepted 2 June 2026; published 3 August 2026)

The control of elastic waves on a chip is essential for next-generation signal processing and integrated acoustics. In this Letter, we experimentally demonstrate an on-chip elastic-wave rainbow capture effect. A topological rainbow emerges by introducing pseudomagnetic field and pseudoelectric fields through structural modulation, where the elastic Landau level modes of different frequencies are spatially separated at distinct positions on the same chip. Interestingly, such bulk rainbow can be captured by the topological chiral edge states originated from the pseudo-magnetic field. We directly measure the rainbow distribution and the ensuing rainbow capture of elastic waves in a silicon-based phononic chip. Our Letter establishes a functional bridge between the bulk rainbow and topological edge states, offering new possibilities for designing the multifrequency devices of elastic waves.

DOI: 10.1103/bkg4-9pr4

The advent of the big-data era has significantly increased the demand for precise control of elastic waves in functional devices, enabling the high-density information processing, nondestructive evaluation, and high-sensitivity remote sensing [1–6]. In recent years, the rapid development of topological phononic crystals (PCs) has provided new avenues for flexible manipulation of elastic waves [7–10]. However, the implementation of topological elastic-wave devices still faces enormous challenges compared to conventional optoelectronic systems, due to the intrinsic inertia of elastic waves with respect to external fields [11]. The introduction of pseudo-magnetic fields has provided an alternative avenue to realize the exotic electromagnetic-analog effects in classical waves systems [12–18]. Benefiting from the high controllability in sample fabrication and experimental characterization of elastic wave systems, it is straightforward to generate effects analogous to pseudomagnetic field (PMF) and pseudoelectric field (PEF) by precisely designing the spatial distribution of strain or material parameters within the structure [19–27]. As such, the quantum Hall physics with Landau levels (LLs) and topological chiral edge states can be achieved and manipulated for elastic waves [25–27].

With the progress in elastic-wave manipulate technologies, realizing multifrequency elastic-wave devices has become essential for integrated on-chip applications. In this context, the topological rainbow effect [28–40], first proposed in electromagnetic systems to spatially separate topological modes with different frequencies and behaved as a multifrequency splitting device [28], has been extended to the elastic PCs [41–45]. Exploring the topological rainbow effect for elastic waves will facilitate the development and application of diverse topological elastic-wave devices, such as topological routers, topological high-capacity storages, and on-chip integrated topological surface-wave devices [44,45]. However, to date, investigations into the topological rainbow effect in elastic systems mainly concentrate on rainbow manipulation of edge modes [41–45], which can only trap a limited number of modes localized at the edges. The topological devices enabling rainbow effect of elastic bulk modes remain unexplored. In particular, how to capture the rainbow and utilize them to manipulate elastic wave propagation is still elusive.

In this Letter, we realize the bulk rainbow and demonstrate that it can be captured by topological edge states in on-chip PCs. We first realize the PMF and PEF simultaneously on a silicon chip, where the PMF gives rise to bulk LLs while the PEF lifts the degeneracy of the LLs to different frequencies, thereby forming the bulk rainbow. Concurrently, the PMF induces topological chiral edge states at the open boundaries, similar to the quantum Hall edge modes. We then directly observe the rainbow distribution of elastic LLs, and more importantly, visualize that the topological chiral edge states can capture the LL rainbow. The edge state at a fixed frequency propagates along the edge, penetrates into the bulk and captures the LL

[*]Contact author: dengwy@whu.edu.cn
[†]Contact author: jylu@whu.edu.cn
[‡]Contact author: phxqhuang@scut.edu.cn
[§]Contact author: zyliu@whu.edu.cn

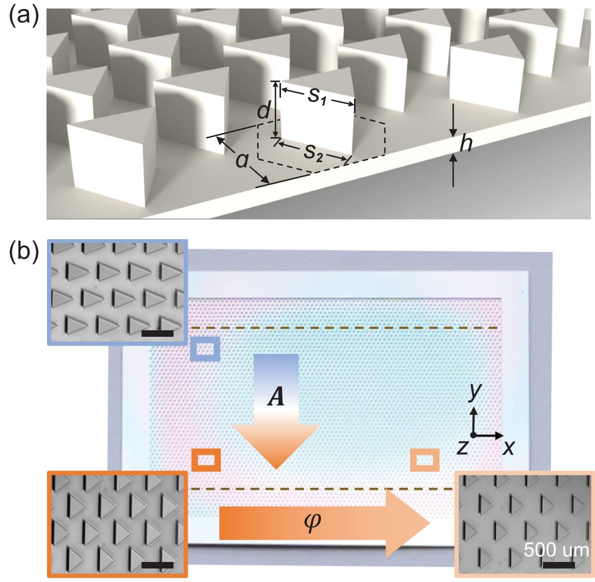

FIG. 1. PMF and PEF on a silicon chip. (a) Schematic of the PC without deformation. The lattice constant $a = 500$ μm, the plate thickness $h = 72$ μm, and the height of triangular pillars $d = 247$ μm. The upper and bottom side lengths of the triangular pillar are $s_1 = 294$ and $s_2 = 0.95 \times s_1 = 279.3$ μm. (b) Photograph of the silicon chip. Both PMF and PEF are engineered by deforming the triangular pillars etched on the top surface of the chip. The brown dashed lines denote the boundaries of the cladding regions. Insets: scanning tunneling microscope images near the upper and bottom boundaries, marked by the blue, orange, and light-orange boxes.

rainbow corresponding to the same frequency, and then exits to the opposite edge. The experimental results are in good agreement with the simulated ones, collectively confirming such rainbow capture effect.

A two-dimensional (2D) PC composed of triangular pillars arranged in a honeycomb lattice embedded in a silicon slab is fabricated by silicon-based technology, as shown in Fig. 1(a). Because of the manufacturing technology, the side length of the regular triangular cross section of the pillar varies in a gradient along the z direction from s_1 to s_2. C_{3v} symmetry guarantees the existence of Dirac conical dispersions at the K and K' points of the first Brillouin zone [24]. When elastic strain is applied to the PC, as shown in Fig. 1(b), a pseudomagnetic or pseudoelectric field will result in the shift of Dirac cone in momentum-frequency space. In order to generate an effective vector potential $\boldsymbol{A}$ in Landau gauge form, a uniaxial deformation along the y direction is constructed. The schematic of deformation is illustrated in Fig. 2(a). Here, ξ is a dimensionless parameter for characterizing the compressing or stretching deformation of the pillar along the y direction with a constant cross section. Keeping the mirror symmetry along the x direction, the Dirac cone shifts along the k_x direction in momentum space, denoted as b_x. The bulk band structures along the high-symmetry lines for three ξ are calculated in Fig. 2(b). It is seen that stretching (brown) and compressing (green) of the pillar induce the Dirac cones to shift away from the K point, as plotted in the inset. To reveal the relation between b_x and ξ, the bulk band structures are simulated where ξ linearly decreases from 1.2 to 0.8, as shown in Fig. 2(c), indicating a linear relationship between b_x and ξ. Then, these deformed pillars are arranged along the y direction, such that b_x is a linear function of y, i.e., $b_x = [-(0.0062/\sqrt{3})y + 0.069](\pi/a)$, acting analogous to a vector potential $\boldsymbol{A} = (b_x, 0, 0)$, which is sensitive to the chirality of the Dirac point. Therefore, a uniform PMF $\boldsymbol{B} = \nabla \times \boldsymbol{A}$ along the z direction is spontaneously generated [46]. To demonstrate the relevant PMF effect, the projected band structure of a ribbon with a gradient deformation along the y direction and periodic boundary condition along the x direction is obtained by both simulation and experiment in Fig. 2(d) [47]. The measured zeroth elastic LL of a flat band is clearly observed near the projection of the K valley, which is well consistent with the simulated result, indicating the successful generation of a uniform PMF.

Subsequently, we consider how to construct a PEF. Biaxial deformation on the pillar is applied to change its filling ratio, as schematically plotted in Fig. 2(e). Here, the scaling factor is denoted by Q. The simulated bulk band structures for three Q exhibit a shift b_0 in Dirac point frequency [Fig. 2(f)]. Specifically, the frequencies of the Dirac point for Q ranging from 0.76 to 0.85 are demonstrated in Fig. 2(g) [47]. When these deformed pillars are arranged along the x direction, b_0 is linearly related to x. So, it effectively provides a scalar potential φ along the x direction, equivalent to generating a uniform PEF $\boldsymbol{E} = -\nabla\varphi$, which affects chirality-dependent dynamics, that is, exerting opposite forces on quasiparticles with different chirality. So far, we have generated PMF and PEF by applying uniaxial and biaxial deformations along the y and x directions, respectively. Therefore, blending these two deformations can simultaneously realize PMF and PEF in a finite structure. To understand the underlying physics, the effective Hamiltonian near the Dirac point can be written as $H_\chi = v_D \boldsymbol{\sigma} \cdot (\boldsymbol{k} + \chi \boldsymbol{A}) + \chi\varphi$, where $\boldsymbol{k}$ are the momenta, v_D is the Dirac velocity, $\boldsymbol{\sigma} = (\sigma_x, \sigma_y, \sigma_z)$ are the Pauli matrices, and $\chi = \pm 1$ represents the chirality corresponding to the K or K' point, respectively. The presence of PMF gives rise to chirality-dependent zeroth LLs. And PEF with different Q induces these degenerate zeroth LLs to shift to different frequencies. The experimental sample is fabricated as shown in Fig. 1(b). The zeroth LLs shift toward higher frequencies as Q decreases [Fig. 2(h)]. Because of the zero group velocities of the zeroth LLs, they will be localized at distinct positions [35], which is expected to achieve rainbow distribution of elastic states.

We calculate the eigenmodes of the finite structure with both PMF and PEF as shown Fig. 3(b), where the in-plane

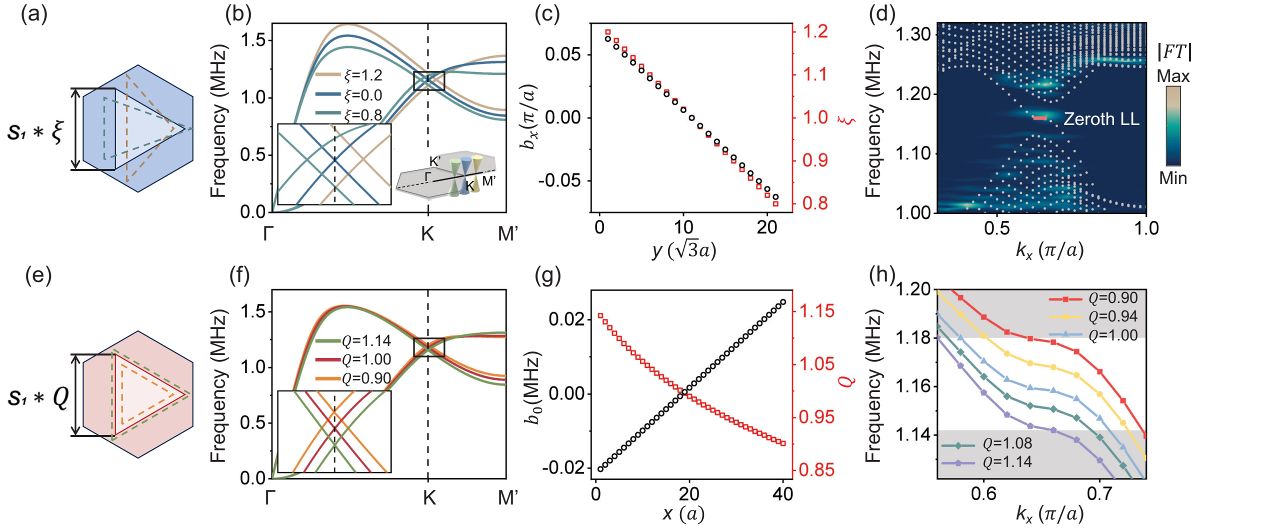

FIG. 2. Deformation-induced PMF and PEF. (a) Uniaxial deformation of triangular pillars generating PMF. ξ characterizes the degree of deformation. (b) Bulk band structures along the high-symmetry lines for $\xi = 0.8$, 0.0, and 1.2, respectively. Left inset: an enlarged view of the band structures within the black box. Right inset: the Dirac cone located originally at the K point with a shift b_x. (c) Evolution of b_x and ξ along the y direction, demonstrating the formation of a uniform PMF. (d) Simulated (white dots) and measured (color map) projected band structures, showing elastic LLs. (e) Biaxial deformation of triangular pillars generating PEF. Q represents the scaling factor. (f) Bulk band structures for $Q = 0.90$, 1.00, and 1.14, respectively. Inset: an enlarged view of the band structure within the black box. (g) Simulated Dirac cone shifts in frequency b_0 (black circles) and Q (red circles) along the x direction. (h) Zeroth LL distributions induced by PEF for $Q = 0.90$, 0.94, 1.00, 1.08, and 1.14, respectively.

mode-dominated bands have been filtered out. The red circles represent the zeroth LLs under PEF, resulting in a continuous frequency distribution determined by the range of Q in the structure. In experiment, an elastic-wave measurement platform is built, as shown in Fig. 3(a), to observe the rainbow distribution of the zeroth LL modes. A tungsten needle, connected to a piezoelectric transducer at the end, is placed on the top surface of the sample to excite elastic wave. A laser Doppler vibrometer mounted on a 3D translation stage is used to detect the out-of-plane component $|u_z|^2$ of the elastic field. Detailed information about the experimental setup is described in [47]. The field distributions of the zeroth LL modes [red circles in Fig. 3(b)] are measured in Fig. 3(c). They are spatially separated and localized at different positions in the sample. The higher the frequency, the more localized the field is to the right side of the sample. The corresponding simulated results are consistent well with the experimental ones, as demonstrated in Fig. 3(d). Thus, the rainbow distribution has been confirmed by both simulation and experiment. It should be mentioned that, due to the manufacturing tolerances, the s_2 of the fabricated sample is found to be slightly smaller than the designed value, which results in a frequency shift of 0.004 MHz between the experimental and simulated results [47].

We have demonstrated that the zeroth LL modes are localized at different positions to exhibit the rainbow effect, and now we use the edge states to capture these rainbow modes, manipulating the elastic wave propagation. As shown in Fig. 2(h), the modes connected to the zeroth LLs are topological edge states induced by PMF, which are analogous to quantum Hall edge states. To confine the edge states and fill the absorbing material, cladding layers composed of eight layers of rotated regular triangular pillars are added to the upper and bottom boundaries of the structure as illustrated in the left panel of Fig. 4(a). The group velocities of these edge states can be manipulated by adjusting the rotation angle of the pillars in the cladding layers [47]. Here, the cladding layers with 30° rotated pillars are selected on both the upper and bottom boundaries. In the absence of PEF, the projected band structure is calculated in the middle panel of Fig. 4(a). For the edge modes of the same valley (e.g., the K' valley), they exhibit chiral transport, that is, the edge states with opposite group velocities are spatially separated on opposite boundaries, as simulated in the right panel of Fig. 4(a). In the presence of PEF, the zeroth LLs split into multiple zeroth LLs distributed at different positions. A sample with a size of 41×80 unit cells is fabricated. The excitation needle is fixed at the upper left boundary, as marked by the green star, and its excitation frequency covers the frequencies of the zeroth LL and related edge state. The edge states with positive group velocity are stimulated and propagate to the right at the upper boundary. Because of the localization of the zeroth LL modes at different positions, the edge states of different frequencies can couple with different zeroth LL modes. This leads to the edge states can only propagate a certain distance on the upper boundary. Then, they transport towards the bottom boundary. Because of the negative group velocities of the edge states on the bottom boundary [middle panel in Fig. 4(b)], they will eventually propagate

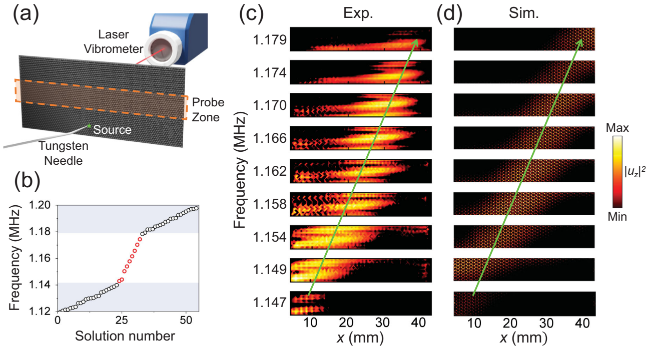

FIG. 3. Experimental observation of rainbow distribution. (a) Schematic of the experimental setup. (b) Simulated eigenmode distributions of the finite sample. The white region indicates the rainbow mode distribution, which is determined by the frequencies of the zeroth LL corresponding to the maximum and minimum Q. (c),(d) Experimental and simulated rainbow distribution for different frequencies at different positions, corresponding to the red circles in (b), respectively.

to the left. The realization of this process is ensured by the combined effect of frequency matching and mode overlap mechanisms, while its transmission efficiency is strongly influenced by the degree of overlap between the edge states and the zeroth LL modes [47]. The measured wave propagations at three different frequencies are collected in Fig. 4(b), clearly capturing the rainbow distribution at three different positions. The corresponding simulated results are illustrated in Fig. 4(c), which agree well with the experimental ones. Moreover, a 2D Fourier transformation of the field within the green dashed region in Fig. 4(b) has been performed, as shown in Fig. 4(d). This Fourier spectrum reveals the momentum-space distribution of the edge states in the Brillouin zone [24]. It is found that only three bright spots are exclusively localized near the K' point, confirming that the observed edge states originate from the projection of the K' valley. Specifically, these states are composed of linear combinations of degenerate basis states associated with the K' valley and are therefore protected by valley topology [49]. In other words, these edge states exhibit negligible intervalley scattering into the K valley during propagation, which underlies their robust transport characteristics [47]. Moreover, some samples with defects and disorders near the bottom cladding, as well as random displacements in each scatterer, are fabricated. The measured waves do not exhibit backscattering during propagation, which further confirms the robustness of rainbow capture. [47]. It is worth noting that by changing the rotation of the pillars in the cladding layers, the wave propagation of the edge state can be manipulated accordingly [47].

In conclusion, we have realized a silicon-chip platform that supports orthogonal PMF and PEF, enabled by the

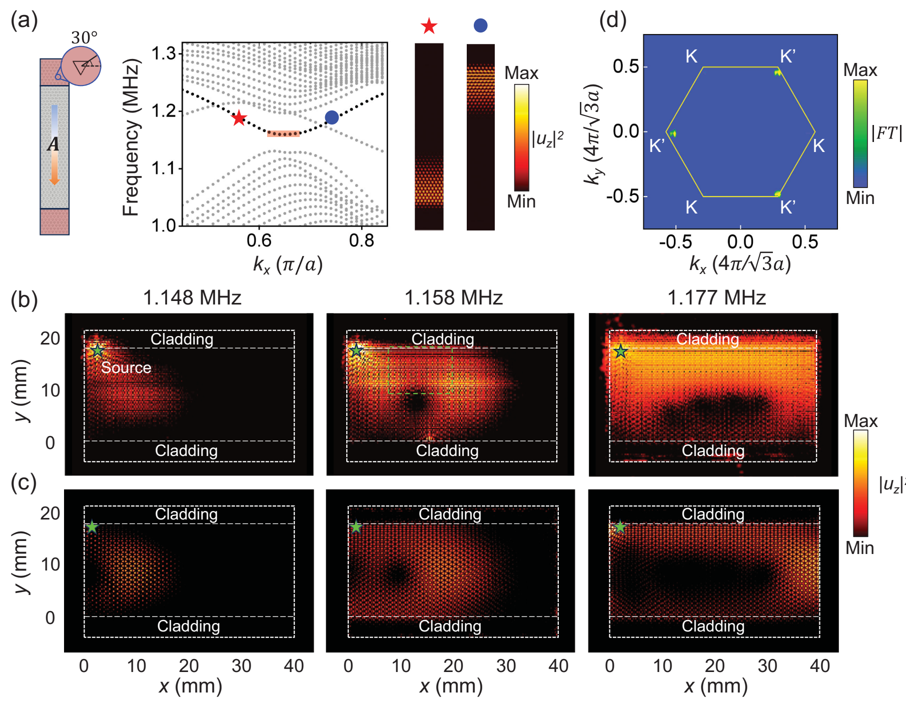

FIG. 4. Rainbow capture. (a) Left panel: Schematic of the structure with cladding layers composed of eight layers of triangular pillars. The pillars at the upper and bottom layers are rotated by 30°. Middle panel: Projected band structure of a ribbon in (a) in the absence of a PEF. Right panel: the eigen field distributions marked by the red star and blue circle in the middle panel, respectively. (b),(c) Measured and simulated displacement field $|u_z|$ excited by a needle source (green star) in the upper left corner near the cladding layer at a frequency of 1.148, 1.158, and 1.177 MHz, respectively. (d) Fourier transformation of the measured displacement field mark by the green box in (b). The yellow hexagon indicates the first Brillouin zone.

flexibility of silicon microfabrication and the intrinsically low dissipation of the chip-based device. The elastic LLs induced by the PMF, become separated in both frequency and real space under the influence of the PEF, giving rise to the rainbow distribution of elastic waves. Notably, such LL rainbow can be captured by the topological chiral edge states similar to the quantum Hall edge modes. The LLs, bulk rainbow and rainbow capture effect have been observed in the on-chip PCs. By introducing active control mechanisms, such as piezoelectric modulation of local parameters, the proposed structure may enable more flexible control over the edge state group velocity, opening opportunities for dynamically reconfigurable topological waveguide devices [50,51].

Note added—A companion letter reporting the similar results on elastic-wave Landau rainbows has been published as Ref. [52].

Acknowledgments—This work was supported by the National Key R&D Program of China (No. 2022YFA1404500, No. 2022YFA1404900, and No. 2023YFB2804701), the National Natural Science Foundation of China (No. 12574519, No. 12374409 and No. U25D8001).

Data availability—The data that support the findings of this article are openly available [47].

[1] W. Zhu, W. Deng, Y. Liu, J. Lu, H.-X. Wang, Z.-K. Lin, X. Huang, J.-H. Jiang, and Z. Liu, Topological phononic metamaterials, Rep. Prog. Phys. **86**, 106501 (2023).

[2] S.-Y. Yu, X.-C. Sun, X. Ni, Q. Wang, X.-J. Yan, C. He, X.-P. Liu, L. Feng, M.-H. Lu, and Y.-F. Chen, Surface phononic grapheme, Nat. Mater. **15**, 1243 (2016).

[3] D. Hatanaka, I. Mahboob, K. Onomitsu, and H. Yamaguchi, Phonon waveguides for electromechanical circuits, Nat. Nanotechnol. **9**, 520 (2014).

[4] B. J. Ash, S. R. Worsfold, P. Vukusic, and G. R. Nash, A highly attenuating and frequency tailorable annular hole phononic crystal for surface acoustic waves, Nat. Commun. **8**, 174 (2017).

[5] J. Cha and C. Daraio, Electrical tuning of elastic wave propagation in nanomechanical lattices at MHz frequencies, Nat. Nanotechnol. **13**, 1016 (2018).

[6] J. Qi, Z. Chen, P. Jiang, W. Hu, Y. Wang, Z. Zhao, X. Cao, S. Zhang, R. Tao, Y. Li, and D. Fang, Recent progress in active mechanical metamaterials and construction principles, Adv. Sci. **9**, 2102662 (2022).

[7] K. H. Matlack, M. Serra-Garcia, A. Palermo, S. D. Huber, and C. Daraio, Designing perturbative metamaterials from discrete models, Nat. Mater. **17**, 323 (2018).

[8] H. Fan, B. Xia, L. Tong, S. Zheng, and D. Yu, Elastic higher-order topological insulator with topologically protected corner states, Phys. Rev. Lett. **122**, 204301 (2019).

[9] M. Serra-Garcia, V. Peri, R. Süsstrunk, O. R. Bilal, T. Larsen, L. G. Villanueva, and S. D. Huber, Observation of a phononic quadrupole topological insulator, Nature (London) **555**, 342 (2018).

[10] G. Ma, M. Xiao, and C. T. Chan, Topological phases in acoustic and mechanical systems, Nat. Rev. Phys. **1**, 281 (2019).

[11] M. O. Goerbig, Electronic properties of graphene in a strong magnetic field, Rev. Mod. Phys. **83**, 1193 (2011).

[12] S. Roy, M. Kolodrubetz, N. Goldman, and A. G. Grushin, Tunable axial gauge fields in engineered Weyl semimetals: Semiclassical analysis and optical lattice implementations, 2D Mater. **5**, 024001 (2018).

[13] V. Peri, M. Serra-Garcia, R. Ilan, and S. D. Huber, Axial-field-induced chiral channels in an acoustic Weyl system, Nat. Phys. **15**, 357 (2019).

[14] L. Tarruell, D. Greif, T. Uehlinger, G. Jotzu, and T. Esslinger, Creating, moving and merging Dirac points with a Fermi gas in a tunable honeycomb lattice, Nature (London) **483**, 302 (2012).

[15] O. Jamadi, E. Rozas, G. Salerno, M. Milićević, T. Ozawa, I. Sagnes, A. Lemaître, L. Le Gratiet, A. Harouri, I. Carusotto, J. Bloch, and A. Amo, Direct observation of photonic Landau levels and helical edge states in strained honeycomb lattices, Light Sci. Appl. **9**, 144 (2020).

[16] Z. Fu, R. Zheng, J. Liang, J. Lu, W. Deng, M. Ke, X. Huang, and Z. Liu, Pseudomagnetic fields in bilayer phononic crystals, Europhys. Lett. **146**, 46004 (2024).

[17] M. Yan, X. Huang, J. Wu, W. Deng, J. Lu, and Z. Liu, Antichirality emergent in type-II Weyl phononic crystals, Phys. Rev. Lett. **130**, 266304 (2023).

[18] Q. Mo, R. Zheng, C. Lu, X. Huang, Z. Liu, and S. Zhang, Observation of oriented Landau levels and helical zero modes in Berry dipole acoustic crystals, Phys. Rev. Lett. **134**, 116604 (2025).

[19] R. Ilan, A. G. Grushin, and D. I. Pikulin, Pseudo-electromagnetic fields in 3D topological semimetals, Nat. Rev. Phys. **2**, 29 (2020).

[20] Y. Chen, Z. Lan, L. Fan, S. Liang, L. An, J. Zhu, and Z. Su, Realization of broadband ultrasonic chiral Landau levels in an elastic metamaterial, Phys. Rev. B **111**, 184303 (2025).

[21] Z. D. Zhang, M. H. Lu, and Y. F. Chen, Observation of free-boundary-induced chiral anomaly bulk states in elastic twisted kagome metamaterials, Phys. Rev. Lett. **132**, 086302 (2024).

[22] C.-R. Mann, S. A. R. Horsley, and E. Mariani, Tunable pseudo-magnetic fields for polaritons in strained metasurfaces, Nat. Photonics **14**, 669 (2020).

[23] J. Cha, K. W. Kim, and C. Daraio, Experimental realization of on-chip topological nanoelectromechanical metamaterials, Nature (London) **564**, 229 (2018).

[24] M. Yan, J. Lu, F. Li, W. Deng, X. Huang, J. Ma, and Z. Liu, On-chip valley topological materials for elastic wave manipulation, Nat. Mater. **17**, 993 (2018).

[25] M. Yan, W. Deng, X. Huang, Y. Wu, Y. Yang, J. Lu, F. Li, and Z. Liu, Pseudomagnetic fields enabled manipulation of on-chip elastic waves, Phys. Rev. Lett. **127**, 136401 (2021).

[26] S. Li, P. G. Kevrekidis, and J. Yang, Emergence of elastic chiral Landau levels and snake states, Phys. Rev. B **109**, 184109 (2024).

[27] Z. Cui, C. Wu, Q. Wei, M. Yan, and G. Chen, On-chip elastic wave manipulations based on synthetic dimension, Phys. Rev. Lett. **133**, 256602 (2024).

[28] S. E. Soliman, M. Barlou, Z. J. Wong, and K. L. Tsakmakidis, Topological rainbow trapping, Nat. Rev. Phys. **7**, 409 (2025).

[29] K. L. Tsakmakidis, A. D. Boardman, and O. Hess, 'Trapped rainbow' storage of light in metamaterials, Nature (London) **450**, 397 (2007).

[30] J. Christensen, P. Huidobro, L. Martin-Moreno, and F. J. Garcia-Vidal, Confining and slowing airborne sound with a corrugated metawire, Appl. Phys. Lett. **93**, 083502 (2008).

[31] G. J. Chaplain, J. M. De Ponti, G. Aguzzi, A. Colombi, and R. V. Craster, Topological rainbow trapping for elastic energy harvesting in graded Su-Schrieffer-Heeger systems, Phys. Rev. Appl. **14**, 054035 (2020).

[32] E. Skelton, R. Craster, A. Colombi, and D. Colquitt, The multi-physics metawedge: Graded arrays on fluid-loaded elastic plates and mechanical analogues of rainbow trapping, New J. Phys. **20**, 053017 (2018).

[33] B. Wilks, F. Montiel, and S. Wakes, Rainbow reflection and broadband energy absorption of water waves by graded barrier arrays, J. Fluid Mech. **941**, A26 (2022).

[34] A. Colombi, D. Colquitt, P. Roux, S. Guenneau, and R. V. Craster, A seismic metamaterial: The resonant metawedge, Sci. Rep. **6**, 27717 (2016).

[35] W. Zhao, Y. Zheng, C. Lu, Z. Wang, Y. C. Liu, and S. Zhang, Landau rainbow induced by artificial gauge fields, Phys. Rev. Lett. **133**, 233801 (2024).

[36] N. AbdelAll, M. Almokhtar, G. Khouqeer, I. Abood, and S. El Soliman, Rainbow trapping with engineered topological corner states and cavities in photonic crystals, Adv. Quantum Technol. **7**, 2400050 (2024).

[37] X. W. Sun, M. T. Tan, G. G. Xu, Y. Cao, X. D. Wen, and Z. J. Liu, Sub-wavelength topological boundary states and rainbow trapping of local-resonance phononic crystal plate, J. Phys. D **57**, 225302 (2024).

[38] A.-Y. Guan, Z.-Z. Yang, W.-J. Yang, S.-F. Li, X.-Y. Zou, and J.-C. Cheng, Controlling sound wave propagation in topological crystalline insulators and rainbow trapping, Phys. Rev. Appl. **18**, 044054 (2022).

[39] C. Lu, Y.-Z. Sun, C. Wang, H. Zhang, W. Zhao, X. Hu, M. Xiao, W. Ding, Y.-C. Liu, and C. T. Chan, On-chip nanophotonic topological rainbow, Nat. Commun. **13**, 2586 (2022).

[40] S. Zhang, Y. Zeng, X. Hong, W. Zhao, Y. Li, W. Guo, Y. Liu, Z. Cui, L. Deng, Z. Guan, G. Zheng, J. Tao, G. Liang, S. Yu, Q. J. Wang, C. T. Chan, and C. Lu, Topological nanorainbow laser, Sci. Adv. **11**, eady6039 (2025).

[41] B. Ungureanu, M. P. Makwana, R. V. Craster, and S. Guenneau, Localizing elastic edge waves via the topological rainbow effect, Phys. Rev. Appl. **15**, 014057 (2021).

[42] H. Fang, G. Xie, H. Huang, and J. Chen, Coupled topological rainbow trapping of elastic waves in phononic crystals, Sci. Rep. **14**, 17011 (2024).

[43] J. Zhao, Q. Wang, X. Wang, W. Yuan, Y. Huang, S. Chen, A. Riaud, and J. Zhou, On-chip valley phononic crystal plates with graded topological interface, Int. J. Mech. Sci. **227**, 107460 (2022).

[44] Y. Chen, L. Fan, J. Zhu, L. An, and Z. Su, Rainbow energy harvesting using a high-order topological meta-device, Nano Energy **127**, 109722 (2024).

[45] Z.-D. Zhang, S.-Y. Yu, M.-H. Lu, and Y.-F. Chen, Gigahertz surface acoustic wave topological rainbow in nanoscale phononic crystals, Phys. Rev. Lett. **133**, 267001 (2024).

[46] B. Graczykowski, M. Sledzinska, F. Alzina, J. Gomis-Bresco, J. S. Reparaz, M. R. Wagner, and C. M. Sotomayor Torres, Phonon dispersion in hypersonic two-dimensional phononic crystal membranes, Phys. Rev. B **91**, 075414 (2015).

[47] See Supplemental Material at http://link.aps.org/supplemental/10.1103/bkg4-9pr4 for realization of uniform pseudomagnetic field by uniaxial deformation, realization of uniform pseudoelectric field by biaxial deformation, simulated and experimental methods, influence of fabrication imperfections, cladding for manipulating edge states, capture mechanism of bulk Landau rainbow modes by edge states, and robustness of the edge states transportation and Landau rainbow mode, which includes Refs. [25,48].

[48] X. Wen, C. Qiu, Y. Qi, L. Ye, M. Ke, F. Zhang, and Z. Liu, Acoustic Landau quantization and quantum-Hall-like edge states, Nat. Phys. **15**, 352 (2019).

[49] J. Lu, C. Qiu, L. Ye, X. Fan, M. Ke, F. Zhang, and Z. Liu, Observation of topological valley transport of sound in sonic crystals, Nat. Phys. **13**, 369 (2017).

[50] P. Dorin and K. W. Wang, Broadband frequency and spatial on-demand tailoring of topological wave propagation harnessing piezoelectric metamaterials, Front. Mater. **7**, 602996 (2021).

[51] Y. Wang, X. Xu, and L. Li, Advances in tunable bandgaps of piezoelectric phononic crystals, Materials **16**, 6285 (2023).

[52] Y. Chen, Z. Lan, X. Wen, and J. Zhu, preceding Letter, Visualization of elastic flat Landau rainbow, Phys. Rev. Lett. **137**, 066601 (2026).